Am J Transl Res 2020;12(2):428-446
www.ajtr.org /ISSN:1943-8141/AJTR0102051

Original Article

Fenofibrate-induced mitochondrial dysfunction and metabolic reprogramming reversal: the anti-tumor effects in gastric carcinoma cells mediated by the PPAR pathway

Lulu Chen[1,2,3,4], Jin Peng[1,3,4], You Wang[1,3,4], Huangang Jiang[1,3,4], Wenbo Wang[1,3,4], Jing Dai[1,3,4], Meng Tang[1,3,4], Yan Wei[1,3,4], Hao Kuang[1,3,4], Guozeng Xu[1,3,4], Hui Xu[1,3,4], Fuxiang Zhou[1,3,4]

[1]Department of Radiation and Medical Oncology, Zhongnan Hospital of Wuhan University, Wuhan 430071, China; [2]Cancer Center, Renmin Hospital of Wuhan University, Wuhan 430060, China; [3]Hubei Province Key Laboratory of Tumor Biological Behaviors, Wuhan 430071, China; [4]Hubei Cancer Clinical Study Center, Wuhan 430071, China

Received September 8, 2019; Accepted December 20, 2019; Epub February 15, 2020; Published February 28, 2020

Abstract: Cancer cells reprogram their metabolism to adapt to fast growth and environmental demands, which differ them from normal cells. Mitochondria are central to the malignant metabolism reprogramming process. Here, we report that PPARα was highly expressed in gastric cancer tissues and negatively correlated with prognosis. Fenofibrate, a common drug used to treat severe hypertriglyceridemia and mixed dyslipidemia, reversed cellular metabolism and mitochondrial dysfunction in gastric cancer cells through PPARα. Our results show that fenofibrate altered glucose and lipid metabolism, inhibited gastric cancer cell proliferation, and promoted apoptosis in gastric cancer cells. We further show that fenofibrate induced mitochondrial reprogramming via CPT1 and the fatty acid oxidation pathway, as well as by activating the AMPK pathway and inhibiting the HK2 pathway. Additionally, fenofibrate inhibited subcutaneous gastric cancer cell tumor growth without obvious toxicity in mice. Collectively, our results indicate that fenofibrate exhibits anti-tumor activity *in vitro* and *in vivo* via the mitochondria and metabolic reprogramming, demonstrating that mitochondrial regulation and the normalization of cancer cell metabolism are novel therapeutic strategies for cancer.

Keywords: Fenofibrate, gastric cancer, PPARα, mitochondrial dysfunctions, metabolic reprogramming

Introduction

It has been long accepted that cancer cells harbor very specific metabolic features mainly characterized by the Warburg effect: anaerobic glycolysis, a tendency to accumulate lipids as substrates for malignant growth, and dysfunctional mitochondria to adapt to an altered microenvironment [1-3]. Therefore, targeting metabolic alterations and abnormal mitochondria, which differentiate cancer cells from normal cells, offers a therapeutic strategy against cancer with potentially fewer side effects in normal cells [3, 4].

Multiple reports indicate a beneficial role for lipid-lowering drugs as anticancer agents [5-10], including fibrates and statins. For example, a ten-year all-cause mortality study revealed that fibrates could significantly lower total mortality and reduced the cancer-related death rate [11]. Fenofibrate (Fen), a potent agonist of peroxisome proliferator-activated receptor alpha (PPARα), has been a commonly used lipid-lowering drug since its clinical introduction in 1975 [12]. PPAR-alpha is a nuclear receptor protein encoded by the PPARA gene in humans. The effects of Fen in treating hypercholesterolemia and hyperlipidemia are believed to be mediated through its stimulation of PPARα [12-14]. Interestingly, recent studies show that fenofibrate may have anti-tumor effects by directly attenuating tumor growth. Anna Wilk *et al*. reported that fenofibrate accumulated in the mitochondrial fraction of human glioblastoma cells, causing sudden and severe inhibition of mitochondrial respiration [15]. Han Dongfeng *et al*. showed that fenofibrate inhibited glycolysis

in glioblastoma cells [16], and Su Cunjin *et al*. reported that fenofibrate suppressed human neuroblastoma cell proliferation and migration via oxidative stress [17].

These findings indicate that fenofibrate might possess anti-tumor activity by regulating mitochondrial function and cellular metabolism. Although fenofibrate displayed anti-tumor effects in glioma, neuroblastoma, lung cancer, prostate cancer, and hepatocellular carcinoma [17-22], its influence on gastric carcinoma has rarely been reported, and its anti-tumor mechanisms remain elusive. Furthermore, the dependency of fenofibrate's anti-tumor effects on PPARα remains controversial [19, 23-26]. This study was designed to verify whether fenofibrate has anti-tumor effects in gastric cancer *in vitro* and to investigate its regulatory roles in mitochondrial function and metabolic reprogramming. In addition, the participation of PPARα toward fenofibrate activity was also studied. We then examined the effectiveness and safety of fenofibrate *in vivo* to demonstrate potentially new approaches and targets in the treatment of gastric cancer.

Materials and methods

Cell lines and animals

Human gastric cancer cell lines MGC803 and SGC7901 were purchased from the China Center for Type Culture Collection (CCTCC). Cells were cultured in DMEM media at 37°C and 5% CO_2. Animal experiments were performed in accordance with the National Institutes of Health Guide for the Care and Use of Laboratory Animals and were approved by the Institutional Animal Care and Use Committee of Zhongnan Hospital, Wuhan University. BALB/c nude mice (male, 6 weeks old) were obtained from Beijing Huafukang Bioscience Co. Inc. (Beijing, China). Mice were housed at room temperature with free access to food and water in the Animal Biosafety Level 3 Laboratory of Wuhan University. After a 1-week acclimation period, the mice were subcutaneously injected into their backs with 0.1 mL of MGC803 cells (3.0×10^6 cells/mL). When tumors reached an average diameter of 5-6 mm, tumor-bearing mice were assigned randomly to different groups. Tumor growth was measured every 3 days. The longest (a) and shortest (b) tumor diameters were determined with a caliper, and tumor volume (V) was calculated as: $V = (a \times b^2)/2$.

CCK8 cell proliferation assay

MGC803 and SGC7901 cell proliferation were determined using the CCK8 assay. MGC803 and SGC7901 cells in logarithmic growth phase were seeded at 4×10^3 cells/well and 2×10^4 cells/well, respectively, in 96-well plates and cultured in 100 μL culture media, with six parallel wells for each sample. To test different concentrations of fenofibrate on gastric cancer cell survival, 0, 12.5, 25, 50, 100, 200, and 400 μM fenofibrate were used to treat MGC803 and SGC7901 cells for 24 h. For detecting the effects of fenofibrate on gastric cancer cell proliferation over time, MGC803 and SGC7901 cells were incubated with 50 μM fenofibrate for 1, 2, 3, 4, or 5 days. At the end of treatment, 100 μL of CCK-8 working solution was added to each well, and plates were incubated at 37°C for 2 h. The absorbance value (OD) of each well was measured at 450 nm using a 96-well plate reader.

Quantitative reverse transcription polymerase chain reaction (qRT-PCR) analysis

qRT-PCR analysis was performed to detect relative mRNA expression levels. Total RNA was extracted using an RNA extraction kit (QIAGEN) according to the manufacturer's instructions. Reverse transcription was performed using a Vazyme HiScript Q RT SuperMix for qPCR (Vazyme, Nanjing, China) according to the manufacturer's instructions. qRT-PCR was performed using the Vazyme ChamQ SYBR qPCR Master Mix (Vazyme, Nanjing, China). PCR was performed in triplicate and analyzed using the ABI Prism 7500HT fast real-time PCR system (Applied Biosystemst, Foster City, CA). Relative quantification values for each gene were calculated by the $2^{-\Delta\Delta Ct}$ method using β-actin as an internal control. Primers sequences were as follows: mtCOX-I-F, CGC CGA CCG TTG ACT ATT CT, mtCOX-I-R, GGG GGC ACC GAT TAT TAG GG, 265 bp; PPARα-F, ATG GTG GAC ACG GAA AGC C, PPARα-R, CGA TGG ATT GCG AAA TCT CTT GG, 124 bp; β-actin-F, TGG CAC CCA GCA CAA TGA A, β-actin-R, CTA AGT CAT AGT CCG CCT AGA AGC A, 186 bp.

Western blot

Total protein was extracted after treatment and protein concentrations were determined using the Bradford method. Proteins (30 μg) were electrophoresed on 12% SDS polyacrylamide

gels, followed by transfer to a nitrocellulose membrane. Membrane was incubated with the following primary antibodies: β-actin, NUDFS1, NUDFV1, NUDFV2, PKM2, HK2, GLUT1, PDHE1α, PFK, CPT1a, BCL-2, BID, BAX, PI3K p110α, p-AKT, AKT (Protein Tech, China), FASN, ACC2, p-ACC2, Caspase-3, PARP, p-AMPKα, and AMPKα (Cell Signaling Technology Inc., Danvers, MA). Blots were washed with TBST, followed by the addition of secondary antibody goat anti-rabbit IgG-HRP or goat anti-mouse IgG-HRP conjugate (1:2,000, Abcam), and specific bands were visualized by ECL (Beyotime Biotechnology, Shanghai, China). Autoradiographs were recorded onto X-Omat AR film (Eastman Kodak Company, Rochester, NY, USA). The density of bands in the resulting film was quantified by Image J software.

Detection of cell apoptosis by flow cytometry

Cells were seeded into 6-well plates with 2 × 10^5 cells/well for MGC803 and 1 × 10^6 cells/well for SGC7901. After 48 h, harvested cells were washed with cold phosphate-buffered saline (PBS) three times and fixed in 70% ethanol at 4°C overnight. Cells were then treated with 10 μg/mL RNase and stained with 50 μg/mL propidium iodide (PI) for 30 min at room temperature in the dark. For apoptosis analysis, cells were stained using the Annexin V-FITC/PI Apoptosis Detection Kit according to the manufacturer's instructions. Apoptotic cells were detected by BD FACSCalibur™.

Mitochondrial membrane potential (MMP) assessment

MMP was assessed using the JC-1 fluorescent probe (Beyotime Institute of Biotechnology) according to the manufacturer's instructions. Briefly, seeded cells (2.0 × 10^5 cells/well) were pre-treated at the indicated concentrations of test compounds. Cells were incubated with 10 mg/mL JC-1 for 20 min at 37°C in the dark, and images were viewed and scanned under fluorescence microscopy (OLYMPUS, IX73, Japan) at 488-nm excitation and 530 nm emission for green (monomers), and at 543 nm excitation and 590 nm emission for red (aggregates). Three repeated measurements were performed. Fluorescence intensity was measured by Image-Pro Plus software. The fluorescence ratio (JC-1 aggregates/monomer) was used to determine the extent of the mitochondrial depolarization.

Detection of intracellular ROS

Intracellular ROS were detected by an oxidation-sensitive fluorescent probe (DCFH-DA; Beyotime Institute of Biotechnology). After treatment with or without 10 mmol/L N-acetyl-L-cysteine (NAC; Invitrogen, Carlsbad, CA) for 0-12 h, cells were washed twice with PBS. They were then incubated with 10 μmol/L DCFH-DA at 37°C for 20 min according to the manufacturer's instructions. Fluorescence microscopy and BD FACS Calibur were used to detect ROS production with green fluorescence signal under 488-nm excitation wavelength and 525-nm emission wavelength. Cell images were acquired using fluorescence microscopy and intracellular ROS intensity was measured by Image-Pro Plus software. Mean fluorescence values derived from flow cytometry were calculated using FlowJo software, version 6.4.2 (FlowJo, USA).

Determination of the quantities and activity of biochemicals

Enzyme activity assays including NADH CoQ reductase (mitochondrial complex I), HK, PFK, and CPT1, and quantification assays for glucose, free fatty acids (FFAs), LA, TG, and TC were carried out according to the manufacturer's instructions for each assay kit (Cominbio Suzhou, China). Protein quantity was estimated by BCA protein assay kit (Beyotime, China). Results were normalized by protein content in each sample and converted to the percentage of the control group.

Seahorse analyses

The metabolic phenotype and cellular energetics of gastric cancer cells were characterized using the Seahorse XFp Analyzer [27]. MGC803 cells were seeded in 24-well XF24 cell culture plates at a density of 5 × 10^4 cells/well and pre-treated for 24 h. Media were then removed, wells were washed, and cells were incubated for 1 h at 37°C without CO_2 in XF modified DMEM assay medium (Seahorse Bioscience) at pH 7.4 supplemented with 1 mM glutamine, 2.5 mM glucose, 1 mM sodium pyruvate, 0.5 mM carnitine, and 1 mM palmitate complexed with 0.2 mM BSA. For glycolytic tests, the extra-

cellular acidification rate (ECAR) was measured in the basal state (no glucose) or after the injection of 10 mM glucose, 5 μM oligomycin, and 50 mM 2DG (Sigma-Aldrich). ECAR is expressed as mpH/min after normalization to protein content measured with a Pierce BCA Protein Assay (Thermo Fisher Scientific). For mitochondrial stress experiments, the oxygen consumption rate (OCR) was measured in the basal state (1 mM palmitate complexed with 0.2 mM BSA) or after the injection of 5 μM oligomycin, 1 μM FCCP (2-[2-[4-(trifluoromethoxy) phenyl] hydrazinylidene]-propanedinitrile), 5 μM rotenone, and 5 μM antimycin A. OCR is expressed as pmol of O_2/min after normalization to protein content.

ATP concentration detection

A luciferase-based ATP assay kit was used to measure cellular ATP levels (Beyotime Institute of Technology, Nanjing, China). In brief, cells were harvested and lysed with the lysis buffer, followed by centrifugation at 16,000 g for 5 min at 4°C. Finally, the level of ATP was determined by mixing 100 μL of supernatant with 100 μL of luciferase reagent and measured by PerkinElmer EnSpire Microplate Reader (Finland). The obtained values were presented as a relative proportion to control.

Colony formation assay

200 pre-treated MGC803 cells/well were placed into 6-well plates (Beaver). After treatment and 14 days of incubation, visible colonies were fixed with 4% methanol for 30 min and then stained with 0.1% crystal violet for 20 min. Plates were washed three times with water and dried for 1 h at 37°C. Crystal violet absorbed in cells was dissolved in 10% acetic acid. Numbers of colonies that contained at least 50 cells were counted over three biological replicates.

Histology analysis and Immunohistochemistry

Histological screening of tumors was performed by serial analysis of H&E coronal sections. Mouse liver and kidney tissues were fixed in 10% buffered formalin with rehydration through graded ethanol solutions and embedded in paraffin. Tissue sections (5 μm) were stained with hematoxylin and eosin (HE). Paraffin-embedded xenograft tumor sections were incubated with 3% H_2O_2 in methanol for 15 min at room temperature (RT). After washout with distilled water, sections were immersed in PBS for 15 min. Antigen retrieval was conducted with boiling at 100°C for 15 min. Sections were then washed again with PBS three times after cooling down to RT. Sections were incubated with diluted primary antibodies overnight at 4°C. Subsequently, the sections were incubated with a biotinylated secondary antibody at RT for 1 h, then the sections were incubated with ABC-peroxidase for 1 h, washed with PBS, stained with diaminobenzidine for 5 min, and counterstained with hematoxylin. The staining was observed under microscope.

Analyses of blood samples

Alanine transaminase (ALT), aspartate transaminase (AST), blood urea nitrogen (BUN), and creatinine (Cr) levels were measured using the kits indicated above from Changchun Huili Biotech according to manufacturer's protocols.

Statistical analysis

Except noted otherwise, the data are presented as mean ± standard deviation. Statistical comparisons were analyzed by one-way ANOVA and Student's test using SPSS22.0 and GraphPad Prism 6 software. The pathological parameters were compared by chi-squared analysis. Kaplan-Meier analysis was used for survival analysis. The difference was considered to be significant when the *P*-value was < 0.05.

Results

High PPARα expression in gastric cancer tissues negatively correlates with prognosis

The expression of PPARα in gastric cancer tissue was higher than normal gastric epithelial tissue, according to Oncomine database analysis ($P < 0.05$, **Figure 1A**). A Kaplan-Meier plot analysis showed that the prognosis of gastric cancer patients with higher PPARα gene expression was poorer than those with low PPARα gene expression (HR = 1.87, $P < 0.05$, **Figure 1B**). Tissue microarray showed that PPARα expression in gastric cancer tissue was higher than normal gastric tissue ($P < 0.05$, **Figure 1C**). These findings highlight that PPARα is highly expressed in gastric cancer tissues and negatively correlates with prognosis.

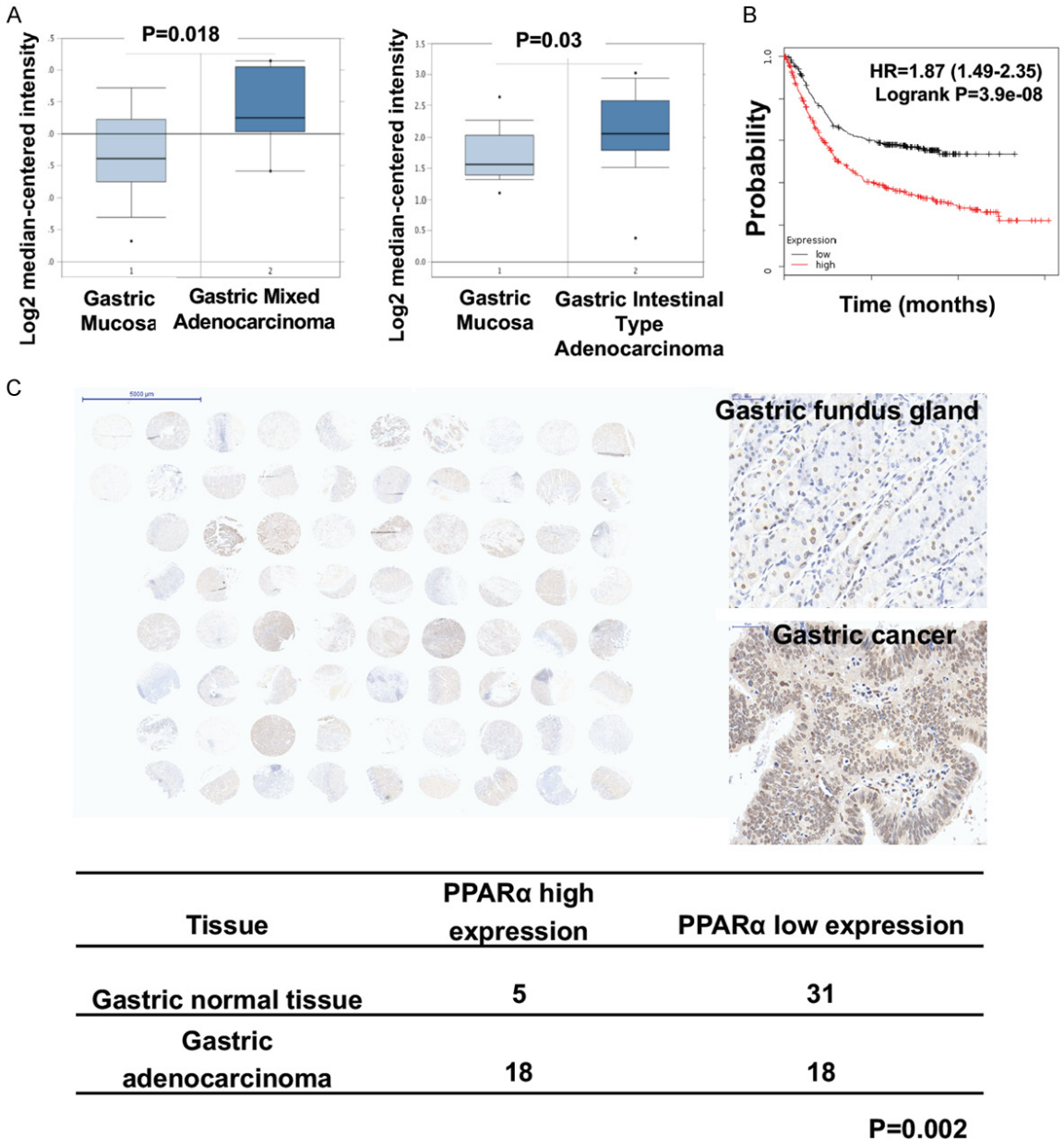

Tissue	PPARα high expression	PPARα low expression
Gastric normal tissue	5	31
Gastric adenocarcinoma	18	18

P=0.002

Figure 1. PPARα was highly expressed in gastric cancer tissues and negatively correlated with prognosis. A. Oncomine database analysis of gene expression of PPARα in gastric mucosa and gastric adenocarcinoma. The expression of PPARα in gastric cancer tissue was higher than that in normal gastric epithelial tissue according to Oncomine database analysis. B. Kaplan-Meier plotter database analysis of the prognosis of patients of gastric cancer with PPARα gene expression levels. C. Representative pictures of PPARα immunohistochemical staining in normal tissues and gastric adenocarcinoma. Analysis of PPARα expression levels of gastric tissue microarray samples. The expression of PPARα was higher in gastric adenocarcinoma than that in gastric normal tissues with significant difference (P = 0.002).

Fenofibrate alters glucose and lipid metabolism in gastric cancer cells through the PPARα pathway

To further explore the anti-tumor mechanisms of fenofibrate, the effect of 50 μM fenofibrate on glycolysis in MGC803 gastric cancer cells was evaluated by Seahorse XF24 analyzer. Fenofibrate treatment reduced MGC803 cell glycolysis. Glycolytic levels for the control and the fenofibrate treatment groups were 82.080 ± 2.717 vs. 68.47 ± 2.179 mPH/min, respec-

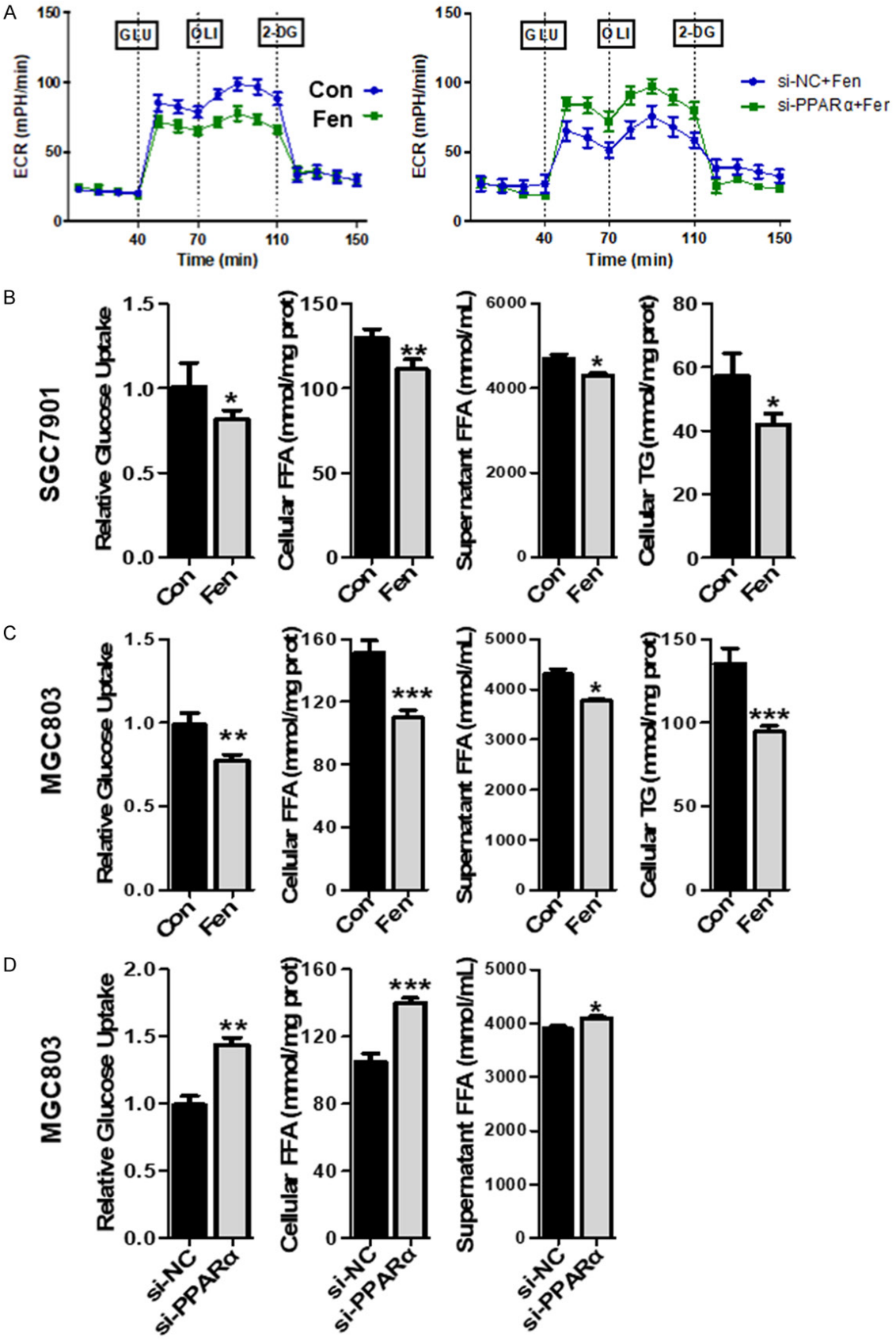

Figure 2. Fenofibrate affected glucose and lipid metabolism in gastric cancer cells through the PPARα pathway. A. The extracellular acidification rate (ECAR) determined by the Seahorse XF24 analyzer in MGC803 cells with or

without fenofibrate treatment. The glycolytic level and glycolysis capacity were calculated from seahorse analysis. PPARα si-RNA interference restored the reduced glycolysis by fenofibrate in MGC803 cells. B and C. Fenofibrate treatment reduced glucose uptake in MGC803 and SGC7901 cells. Compared with the control group, glucose uptake, the free fatty acids in the cell lysate and supernatant and triglyceride decreased after fenofibrate treatment. D. PPARα si-RNA interference restored the inhibition of glucose uptake by fenofibrate in gastric cancer cells. PPARα si-RNA interference restored the cellular and supernatant free fatty acid content decreased by fenofibrate. *indicates when compared to control group $P < 0.05$, **indicates when compared to control group $P < 0.01$, ***indicates when compared to control group $P < 0.001$.

tively ($P < 0.01$). The glycolytic capacity of the control and the fenofibrate treatment group were 93.720 ± 2.296 vs. 72.060 ± 2.126, respectively ($P < 0.001$, **Figures 2A** and S1). Glycolysis values (glycolytic level and glycolytic capacity) of siPPARα combined with fenofibrate treatment were higher than those of the siNC control combined with fenofibrate treatment ($P < 0.01$ and $P < 0.001$, **Figure 2A**) in MGC803 cells. Furthermore, compared with the control group, glucose uptake, FFAs in cell lysate and supernatant, and triglycerides decreased after fenofibrate treatment (**Figure 2B**, **2C**, all $P < 0.05$). Glucose uptake and FFAs in the siPPARα-fenofibrate treatment group were higher than the siNC control-fenofibrate group in MGC803 cells (**Figure 2D**). Collectively, we demonstrated that fenofibrate altered glucose and lipid metabolism in gastric cancer cells through the PPARα pathway.

Fenofibrate inhibits gastric cancer cell proliferation and promotes apoptosis through the PPARα pathway

To explore the influence of fenofibrate on gastric carcinoma, CCK-8 experiments were performed to determine whether fenofibrate significantly inhibited proliferation in the gastric cancer cell lines MGC803 and SGC7901. Its inhibitory effect was enhanced in a concentration- and time-dependent manner. MGC803 cell survival decreased after 24 h of treatment with 25 μM, 50 μM, 100 μM, 200 μM, and 400 μM fenofibrate, whereas SGC7901 cell survival decreased after 24 h of treatment starting at 50 μM fenofibrate (Figure S2A). Compared with the 0 μM control group, 50 μM fenofibrate inhibited MGC803 cell proliferation after 24 h from 1.872 ± 0.089 to 1.565 ± 0.031 (fold change, $P < 0.05$), and from 1.814 ± 0.010 to 1.495 ± 0.005 (fold change, $P < 0.001$) for SGC7901 cells (**Figure 3A**). Compared with the control group, fenofibrate treatment reduced cell density and cell size, widened cell gap, and increased the proportion of detached cells (Figure S2B). Fenofibrate treatment increased apoptosis compared with the control group in MGC803 ($P < 0.001$) and SGC7901 ($P < 0.01$) cells, and the ROS scavenger N-acetylcysteine reduced fenofibrate-induced apoptosis in both MGC803 ($P < 0.001$) and SGC7901 ($P < 0.01$) cells (**Figure 3B**). In MGC803 cells, fenofibrate treatment decreased BCL-2 expression ($P < 0.01$), and increased BID, BAX, cleaved Caspase-3, and cleaved PARP expression significantly (**Figures 3C** and S2C).

In MGC803 cells, PPARα protein expression was decreased by PPARα siRNA (siPPARα) interference ($P < 0.001$ and $P < 0.01$, **Figure 3D**). The apoptosis rate in the siPPARα-fenofibrate treatment group was lower than that of the control siNC-fenofibrate treatment group ($P < 0.05$, **Figure 3E**). The proliferation rates of the siPPARα-fenofibrate group were higher than the siNC-fenofibrate group ($P < 0.01$, **Figure 3F**), and the number of formed clones in cells treated with both GW9662 (PPARα inhibitor) and fenofibrate was higher than fenofibrate alone ($P < 0.01$, **Figure 3G**). These results show that fenofibrate possesses anti-tumor effects in gastric cancer by inhibiting cell proliferation and promoting apoptosis through the PPARα pathway.

Fenofibrate induces mitochondrial reprogramming through CPT1 and the fatty acid oxidation

Mitochondria are critical intracellular organelles that participate in bioenergetic metabolism and cellular homeostasis [28, 29]. The relative values for carnitine palmitoyl transferase 1 (CPT1) activity in the MGC803 cell control group and fenofibrate-treated group were 1.000 ± 0.013 vs. 7.483 ± 0.534, respectively ($P < 0.001$), while for SGC7901 cells, were 1.000 ± 0.02132 vs. 2.877 ± 0.1796 ($P < 0.001$), indicating increased activity in both cell lines (**Figure 4A**). CPT1 activity in the siPPARα-fenofibrate treatment group was higher than

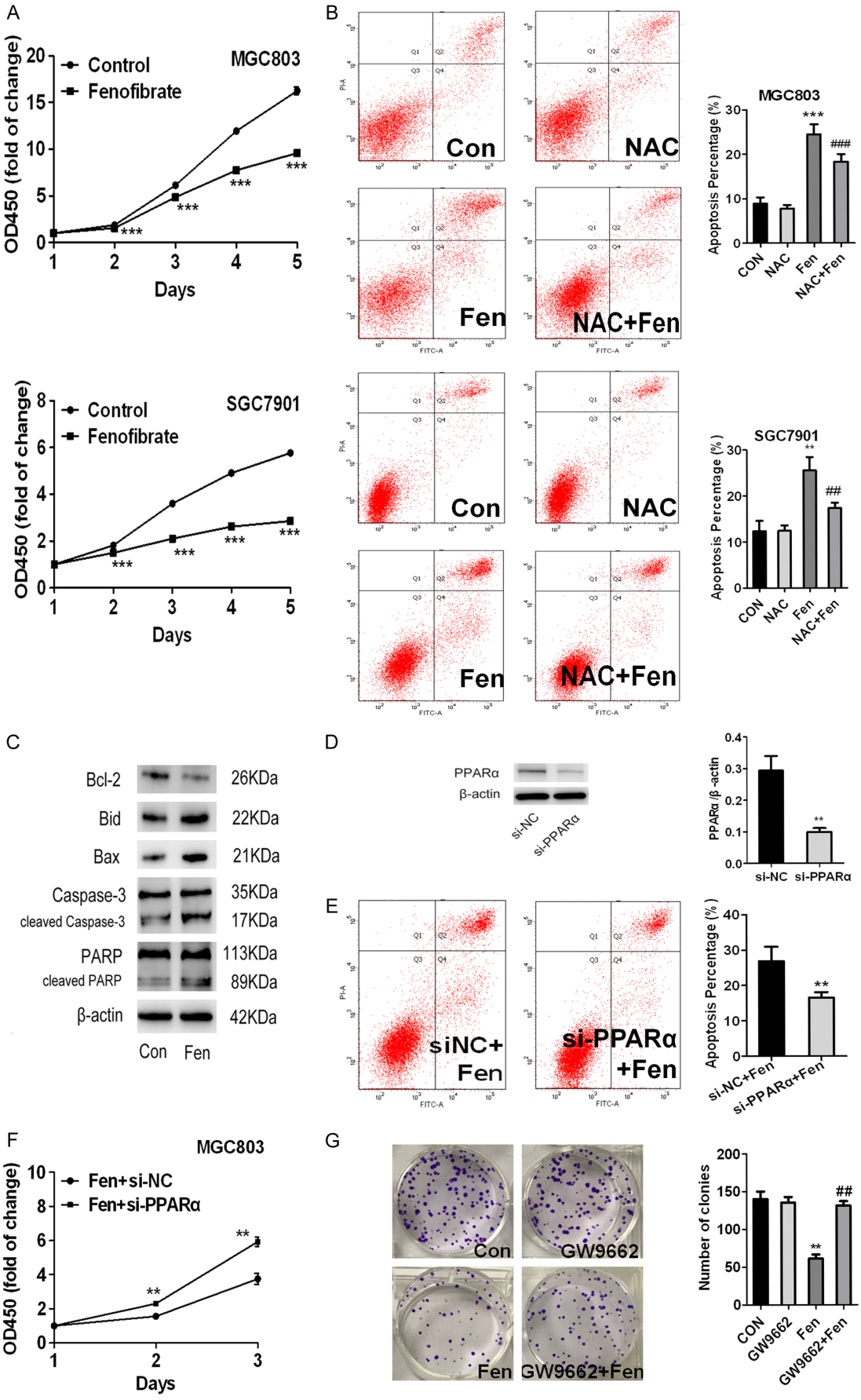
A
MGC803
Control
Fenofibrate
OD450 (fold of change)
Days
SGC7901
B
Con
NAC
Fen
NAC+Fen
Apoptosis Percentage (%)
CON
NAC
Fen
NAC+Fen
C
Bcl-2
Bid
Bax
Caspase-3
cleaved Caspase-3
PARP
cleaved PARP
β-actin
26KDa
22KDa
21KDa
35KDa
17KDa
113KDa
89KDa
42KDa
Con
Fen
D
PPARα
β-actin
si-NC
si-PPARα
PPARα /β-actin
E
siNC+ Fen
si-PPARα +Fen
si-NC+Fen
si-PPARα+Fen
F
Fen+si-NC
Fen+si-PPARα
G
GW9662
Fen
GW9662+Fen
Number of clonies

Figure 3. Fenofibrate inhibited gastric cancer cell proliferation and promoted apoptosis through PPARα pathway. A. Effects of 50 μM fenofibrate treatment on proliferation of MGC803 and SGC7901 cells for different periods of time. B. Flow cytometry analysis of the effect of fenofibrate on apoptosis on MGC803 and SGC7901 cells. Fenofibrate treatment increased apoptosis compared with the control group in MGC803 ($P < 0.001$) and SGC7901 cells ($P < 0.01$), and ROS scavenger N-acetylcysteine reduced fenofibrate-induced apoptosis in MGC803 ($P < 0.001$) and SGC7901 cells. C. Western blot was used to detect the apoptosis-related proteins Bcl-2, Bid, Bax, Caspase3 and PARP protein expression in the control group and fenofibrate treatment group. The gray values of the bands were measured. *indicates when compared to control group $P < 0.05$, **indicates when compared to control group $P < 0.01$, ***indicates when compared to control group $P < 0.001$; ##indicates when compared to fenofibrate treatment group $P < 0.01$, ###indicates when compared to fenofibrate treatment group $P < 0.001$. D. PPARα si-RNA interference decreased PPARα protein levels in MGC803 cells. The gray values of the bands were measured. E. PPARα si-RNA interference reduced the apoptotic percentages of MGC803 cells caused by fenofibrate treatment using Flow cytometry detection method. F. PPARα si-RNA interference partially restored fenofibrate's inhibitory effect on the MGC803 cells proliferation in CCK8 assays. G. In colony formation assay, PPARα inhibitor (GW9662) restored the inhibition of colony formation after fenofibrate treatment in MGC803 cells.

siNC-fenofibrate control in MGC803 cells (**Figure 4A**). The expression levels of the fatty acid metabolism-related proteins FASN and ACC2 decreased, and the expression levels of p-ACC2 and CPT1a protein were increased significantly after fenofibrate treatment (all $P < 0.05$, **Figure 4B**). We next determined the effects of 50 μM fenofibrate treatment on mitochondrial respiration in MGC803 cells using a Seahorse XF24 analyzer. Compared with the control group, mitochondrial respiration decreased significantly after fenofibrate treatment. Basal respiration levels for the control and fenofibrate-treated groups were 905.700 ± 34.120 vs. 389.600 ± 10.600 pmol/min, respectively ($P < 0.001$). ATP production in the control and fenofibrate-treated groups was 439.700 ± 14.440 vs. 247.500 ± 10.830 pmol/min, respectively ($P < 0.001$). The maximal respiratory levels in the control and fenofibrate-treated groups were 1,236.000 ± 46.330 vs. 263.100 ± 10.820 pmol/min, respectively ($P < 0.001$). Mitochondrial respiration levels (basal respiratory level, ATP production, maximal respiratory level) of the siPPARα-fenofibrate group were higher than that of the siNC-fenofibrate control group (**Figures 4C** and S3A).

The activity of mitochondrial complex I in the mitochondrial electron transport chain decreased after fenofibrate treatment in MGC803 and SGC7901 cells. Mitochondrial complex I activity as well as MMP in the siPPARα-fenofibrate treatment group was higher than that of siNC-fenofibrate controls (both $P < 0.05$, **Figure 4D**). The expression of mitochondrial complex I subunits NDUFS1, NDUFV1, and NDUFV2 in MGC803 and SGC7901 cells decreased significantly after fenofibrate treatment (all $P < 0.01$, **Figure 4D**). JC-1 fluorescence was measured by fluorescence microscope to show MMP changes in MGC803 and SGC7901 cells treated with 50 μM fenofibrate for 24 h. The relative MMP (red fluorescence and green fluorescence ratios) in the MGC803 cell control group and fenofibrate treatment group were 39.050 ± 7.778 vs. 0.095 ± 0.010, respectively ($P < 0.01$). The MMP of cells treated with both GW9662 and fenofibrate was higher than that of fenofibrate alone (**Figures 4E** and S3B). Mitochondria became depolarized by fenofibrate, and the MMP decreased. After fenofibrate treatment, ROS green fluorescence intensity and SOD2 increased significantly (both $P < 0.001$, **Figures 4F** and S3C), indicating increased ROS production (Figure S3C). NAC pretreatment partially reduced ROS production caused by fenofibrate. ROS production in the siPPARα-fenofibrate treatment group was less than that of the siNC-fenofibrate control (both $P < 0.01$, **Figure 4G**). Fenofibrate treatment decreased ATP production in MGC803 and SGC7901 cells. The ATP production of the siPPARα-fenofibrate treatment group was greater than the siNC-fenofibrate control ($P < 0.01$ and $P < 0.05$ respectively, **Figure 4H**). Taken together, fenofibrate induces mitochondrial reprogramming through CPT1 and the fatty acid oxidation pathway.

Fenofibrate induces mitochondrial reprogramming by activating the AMPK pathway and inhibiting the HK2 pathway

Cancer cells were believed to primarily utilize glycolysis for ATP production, referred to as the Warburg effect. However, recent evidence suggests that oxidative phosphorylation (OXPHOS) plays a crucial role during cancer progression [30]. Linglin Yu et al. constructed a regulatory network of genes and metabolites from which we extracted a core circuit, containing HIF-1,

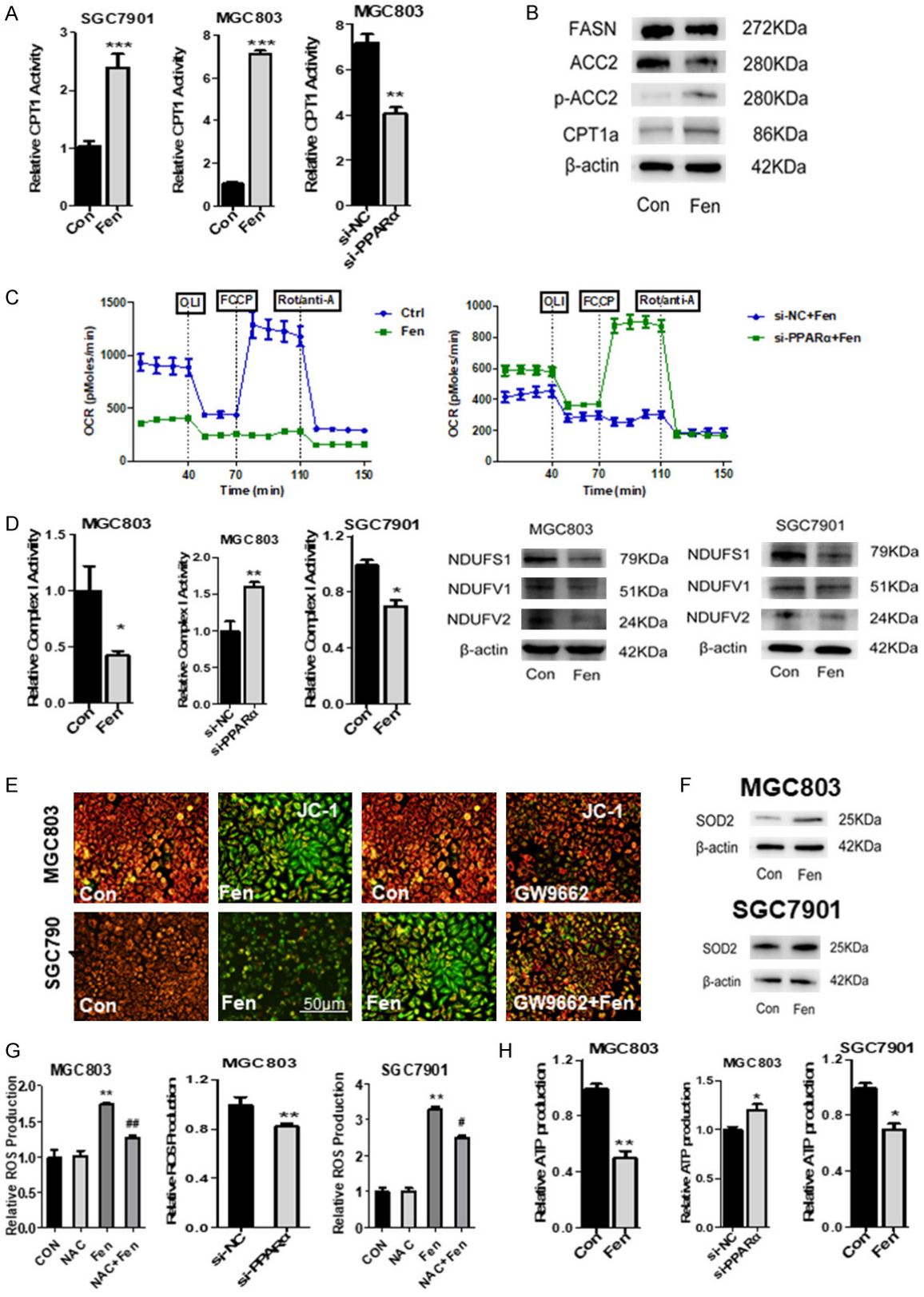

Figure 4. Fenofibrate induced mitochondrial reprogramming through CPT1 and fatty acid oxidation pathway. A. Effects of fenofibrate on the activity of carnitine palmitoyl transferase 1 in gastric cancer MGC803 and SGC7901 cells. PPARα si-RNA interference reduced the carnitine palmitoyltransferase-1 activity increased by fenofibrate in MGC803 cells. B. The expression levels of fatty acid metabolism related proteins FASN and ACC2 were decreased,

and the expression levels of p-ACC2 and CPT1a protein were increased significantly after fenofibrate treatment. C. The oxygen consumption rate (OCR) determined by the Seahorse XF24 analyser in MGC803 cells with or without fenofibrate treatment. Basal respiration level, ATP production and maximal respiration level were calculated from the seahorse analysis. D. Effects of fenofibrate on the mitochondrial complex I activity in gastric cancer MGC803 and SGC7901 cells. Western blot analysis of mitochondrial complex I subunits NDUFS1, NDUFV1, NDUFV2 protein expression in MGC803 and SGC7901 cells with or without fenofibrate treatment. E-G. Effects of fenofibrate on ROS production and SOD2 levels in gastric cancer MGC803 and SGC7901 cells. H. The effects of fenofibrate on ATP production in gastric cancer MGC803 and SGC7901 cells. **indicates when compared to control group P < 0.01, ***indicates when compared to control group P < 0.001.

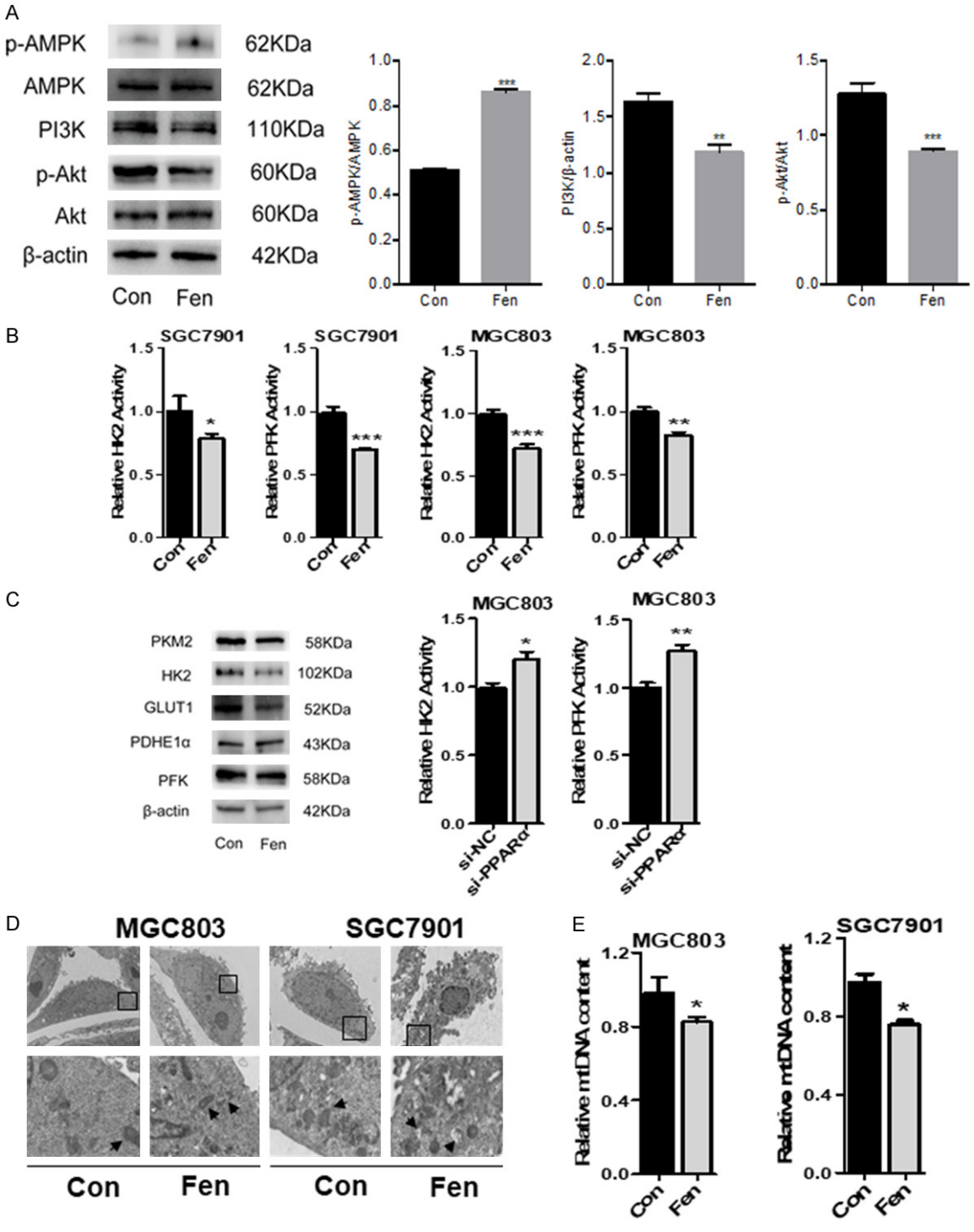

Figure 5. Fenofibrate induced mitochondrial reprogramming by activating the AMPK pathway and inhibiting the HK2 pathway. A. Detection of molecular expression levels of AMPK and PI3K/Akt signaling pathways with or without fenofibrate by Western blot. The results showed that the relative expression of p-AMPK/AMPK protein in MGC803 cells was increased ($P < 0.001$) after fenofibrate treatment, while that of PI3K (β-actin as internal reference protein) and p-Akt/Akt protein decreased ($P < 0.01$ and $P < 0.001$, respectively). B. Effect of fenofibrate on the activity of hexokinase and phosphofructokinase. C. Western blot analysis of glucose metabolism related proteins PKM2, HK2, GLUT1, PDHE1α and PFK expression in gastric cancer MGC803 cells with or without fenofibrate treatment. PPARα si-RNA interference reversed the inhibitory effects of fenofibrate on the activity of hexokinase and phosphofructokinase enzyme activity in MGC803 cells. D. Effects of fenofibrate on the mitochondrial structures of gastric cancer cells under transmission electron microscope. After fenofibrate treatment, the mitochondria of MGC803 cells and SGC7901 cells were depolarized, and the mitochondrial membrane potential decreased. E. Mitochondrial DNA content decreased after 48 hours of 50 μM fenofibrate treatment. *indicates when compared to control group $P < 0.05$, **indicates when compared to control group $P < 0.01$, ***indicates when compared to control group $P < 0.001$.

AMPK, and ROS. In general, cancer cells can have three stable states-a Warburg state (W: high HIF-1, low p-AMPK), an oxidative state (O: low HIF-1, high p-AMPK), and a hybrid state (W/O: high HIF-1, high p-AMPK) [31]. Western blot was used to detect the effects of fenofibrate on the expression of p-AMPK, AMPK, PI3K, p-AKT, and AKT in MGC803 cells after 48 h treatment. The relative expression of p-AMPK/AMPK protein in MGC803 cells was increased ($P < 0.001$) after fenofibrate treatment, while that of PI3K and p-AKT/AKT protein decreased ($P < 0.01$ and $P < 0.001$, respectively) (**Figure 5A**). HK2 and PFK activity in MGC803 and SGC7901 cells decreased significantly after fenofibrate treatment (**Figure 5B**, all $P < 0.05$). After fenofibrate treatment, PDH expression increased, and the expression of PKM2, HK2, GLUT1, and PFK were decreased (all $P < 0.05$, **Figure 5C**). HK2 and PFK activity for the siPPARα-fenofibrate treatment group were higher than siNC-fenofibrate controls in MGC803 cells (**Figure 5C**). Compared with the control group, fenofibrate treatment caused mitochondrial swelling, mitochondrial cristae destruction or disappearance, mitochondrial vacuolization, and mitochondrial pyknosis (**Figure 5D**). Decreased mitochondrial DNA copy number was also observed in the fenofibrate treatment group in both cell lines ($P < 0.05$, **Figure 5E**). These data show that fenofibrate induced mitochondrial reprogramming by activating the AMPK pathway and inhibiting the HK2 pathway.

Fenofibrate inhibits tumor growth in vivo through reversing metabolic reprogramming and apoptosis induction

The subcutaneous tumor-bearing mouse models of MGC803 cells were successfully established. Compared with the control group, the tumors in the fenofibrate-treated group grew more slowly than those in control group (**Figure 6A**), and the tumor weight of the fenofibrate-treated group was lower ($P < 0.05$, **Figure 6B**, **6C**). The number of necrotic cells increased with fenofibrate treatment, while HE staining showed no significant changes in liver and kidney tissue structures in both groups (Figure S4A). No significant differences in liver and kidney indexes (ALT, AST, Cr, BUN) and body weight were observed between control and fenofibrate treatment groups (all $P > 0.05$, Figure S4B, S4C). Compared to controls, in the fenofibrate treatment group, the expression of tumor tissue proliferation indexes (Ki67, PCNA) decreased (both $P < 0.01$, **Figure 6D**), the proportion of TUNEL positive cells and apoptosis indexes (BAX, Caspase-3, cleaved PARP) increased (all $P < 0.001$, **Figure 6E**), and BCL-2 decreased ($P < 0.05$, **Figure 6F**). Additionally, the expression of glucose metabolism indexes (GLUT1, GLUT4, PKM2, HK2, PFK) decreased ($P < 0.05$), while PDH increased ($P < 0.05$, **Figure 6G**), FASN decreased ($P < 0.05$), and the expression of p-ACC and CPT1a increased ($P < 0.05$, **Figure 6H**). SOD2 expression also increased ($P < 0.05$, **Figure 6I**). In conclusion, these data indicate that mitochondria and metabolic reprogramming were targets of fenofibrate, with fenofibrate exhibiting anti-tumor activity both *in vitro* and *in vivo*.

Discussion

Stomach cancer is the fifth most frequently diagnosed cancer and the third leading cause of cancer deaths worldwide [32]. The low rate of early diagnosis results in a large proportion of advanced diseases at the time of diagnosis, reducing the changes for radical surgery. Advanced (clinical stage IV) gastric carcinoma has a median survival of just ~9-10 months [33]. The main treatment for advanced gastric cancer is systematic chemotherapy [4]. How-

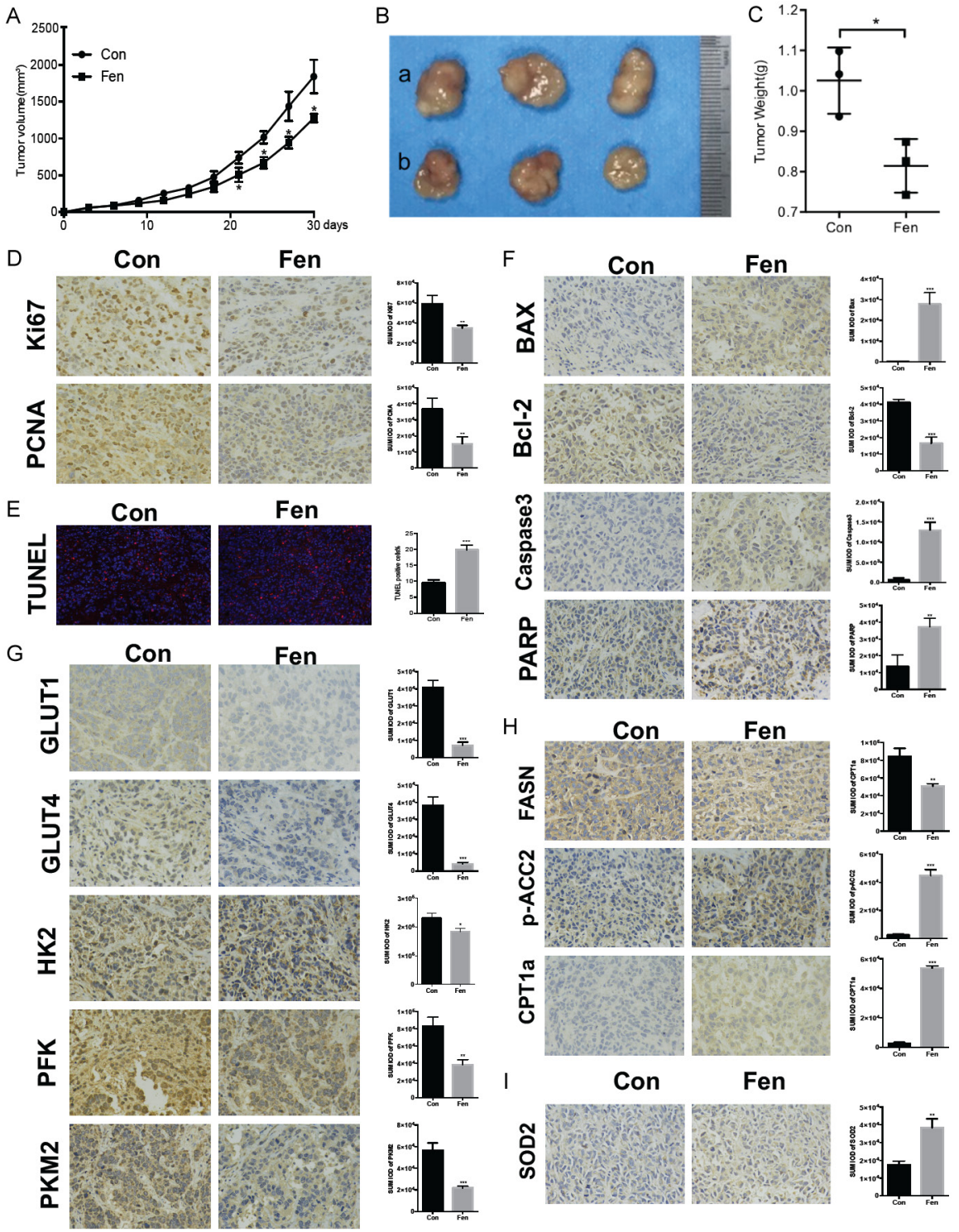

Figure 6. Fenofibrate inhibited tumor growth *in vivo* through metabolic reprogramming reversal and apoptosis induction. (A) Growth curve of tumor volume. Compared with the control group, the tumors of the fenofibrate-treated group grew more slowly than those in control group (B) Gross view of tumor. (C) The tumor weights have a significant statistical difference between control group and fenofibrate treatment group. (D) Representative images of Ki-67 and PCNA IHC staining in tumor tissue. The fenofibrate administration group had less Ki-67 and PCNA expression (brown) than control group. (E) Representative images of TUNEL staining in tumor tissue. The fenofibrate administration group had more DNA leakages (red) than control group. (F) Representative IHC images of Bax, Bcl-2, Caspase3 and PARP in tumor tissue. The fenofibrate group had higher Bax, Caspase3, PARP expression levels and lower Bcl-2

expression level than that of control group. (G) Representative IHC images of GLUT1, GLUT4, HK2, PFK, PKM2 and PDH in tumor tissue. The fenofibrate group had lower GLUT1, GLUT4, HK2, PFK, PKM2 expression levels and higher PDH expression level than that of control group. (H) Representative IHC images of FASN, p-ACC2, and CPT1a in tumor tissue. The fenofibrate group had lower FASN expression level and higher p-ACC2, and CPT1a expression level than that of control group. (I) Representative IHC image of SOD2 in tumor tissue. The fenofibrate group had higher SOD2 expression level than that of control group. The integrated optical densities of different molecules staining were measured, *indicates when compared to control group $P < 0.05$, **indicates when compared to control group $P < 0.01$, ***indicates when compared to control group $P < 0.001$.

ever, patients commonly develop drug resistance and suffer from serious side effects, which can lead to treatment interruption and failure. Therefore, finding effective new strategies and drugs for gastric carcinoma with low toxicity is urgently required. Here, we confirm fenofibrate's anti-tumor activity and mechanistically identify that fenofibrate attenuates tumor growth by regulating mitochondrial function and normalizing cancer cell metabolism, partially through PPARα pathway. Fenofibrate administration *in vivo* also showed anti-tumor effects without obvious systemic toxicity.

We confirmed fenofibrate's anti-tumor effects in the gastric cancer cell lines MGC803 and SGC7901 through attenuated tumor cell growth. Fenofibrate increased the percentage of apoptotic cells and induced pro-apoptotic biomarker expression. Combined with other studies, fenofibrate continues to demonstrate anti-tumor effects in various cancer categories [17-22], indicating a potentially universal anti-tumor mechanism.

Metabolic reprogramming is currently recognized as one of the hallmarks of cancer [34]. It has been shown that carcinogenesis is associated with decreased levels of mitochondrial proteins and the upregulation of glycolytic enzymes [35]. Cancer cells rely on glycolysis to provide substrates for rapid replication. After fenofibrate treatment in gastric cancer cells, glycolysis levels were attenuated by decreased glucose uptake, glycolytic enzyme activity, and regulated expression of glycolysis-related proteins.

Several lines of evidence suggest that targeting *de novo* fatty acid synthesis may be effective in the treatment of some cancers. Fatty acids are a key component of cell membranes and can also either act as signaling molecules or store energy. It was first discovered in the 1950s that tumors were able to synthesize lipids, and a subsequent study determined that most lipids in tumors cells were synthesized *de novo* [36, 37]. Since then, numerous studies have identified *de novo* fatty acid biosynthesis as a key metabolic requirement for some cancers [36, 37]. Except for liver, adipose, and lactating breast tissues, adult tissues do not synthesize fatty acids *de novo* [40], offering the inhibition of *de novo* fatty acid synthesis as a potential therapeutic alternative. Fenofibrate decreased the quantity of FFAs and triglycerides in cells. FASN and ACC were down-regulated, while phosphorylation of ACC enzyme (thus inactivating it) and CPT1 expression were upregulated. CPT1 activity, which transfers FFAs into the mitochondrial matrix and is the first component and rate-limiting step in the beta-oxidation of long-chain fatty acids, increased after fenofibrate treatment, indicating fenofibrate could not only decrease FFA synthesis but also promote its catabolism.

We report that fenofibrate induces mitochondrial dysfunction by decreasing MMP and inducing oxidative stress. It has been known for many years that pro-oxidant conditions induced by mitochondria-derived ROS may contribute to tumorigenesis or sustain tumor progression. In fact, many tumor tissues show higher ROS levels when compared to their normal counterparts [41]. Excessive ROS above a critical threshold was reported to lead to cell death by inducing damage to DNA, lipids, and proteins [42]. Many bioactive agents like cargo-free NP based on cationic lipids and cationic peptides (such as 6K) encapsulated into cNP caused cancer cell death through ROS generation [43, 44]. Fenofibrate increased ROS production significantly and promoted expression of the ROS scavenger SOD2. We further show that fenofibrate promotes cancer cell apoptosis by inducing ROS production, which is mainly derived from mitochondria [45, 46], and significantly decreasing ATP production. A recent study showed that cisplatin-resistant lung adenocarcinoma cells exhibited higher MMP and ATP lev-

els, which confer migratory and invasive capabilities to these cells [47]. New evidence suggests ATP production (bioenergetics) and apoptosis (cell life/death decision) have a more intimate link than previously thought, mediated by the remodeling of the mitochondrial ultrastructure during apoptosis [48].

Fenofibrate treatment diminished mitochondrial OXPHOS by decreasing OCR, mitochondrial complex I activity, and protein subunit expression. Because OXPHOS is crucial for anchorage-independent cancer cell proliferation [49], the inhibition of OXPHOS can effectively inhibit tumor migration and invasion [50]. Targeting mitochondria, which are necessary for the electron transport chain and OXPHOS, starves cancer cells of ATP and limits the growth and metastasis of tumors [51]. Genes that encode complex I subunits are associated with mitochondrial OXPHOS and the electron transport chain [52], and complex I was reported to be an anti-tumor target [53]. Healthy cells can maintain functionality even in the presence of mitochondrial inhibitors, making these targets viable as treatment options [51]. Several treatments have been shown to interfere with normal mitochondrial function in lung tumor cells, including metformin, BAY87-2243, and microRNA-126 [54-57]. These treatments target different aspects of mitochondrial function. For example, metformin reduces oxygen consumption in the presence of pyruvate and malate, starving mitochondrial complex I of its substrate, NADH. Metformin may also disrupt lipid metabolism, glucose metabolism, tricarboxylic acid cycle, the methionine cycle, the folate cycle, and nucleotide synthesis [58-61].

Abnormalities in the PI3K/AKT pathway are closely related to tumorigenesis, progression, and drug resistance. Inhibition of PI3K/AKT can result in the inhibition of tumor cell growth and programmed cell death [62]. In a state of energy deprivation, AMPK activates fatty acid oxidation and blocks metabolic processes such as cholesterol biosynthesis, while AMPK is a potent inhibitor of glycolysis [63]. The present study found that fenofibrate promotes the expression of p-AMPKα (Thr172) (thus activating) and inhibits the expression of PI3K and p-AKT (Ser 473) (thus inactivating). Fenofibrate might inhibit the malignant transformation of tumors by regulating these tumor cell signaling pathways.

Due to either high energetic and oxidative stress or the activation of specific oncogenes, cancer cells can be in a hybrid metabolic phenotype, utilizing both glycolysis and OXPHOS. Because cells in the hybrid 'W/O' state have increased plasticity, they could have an advantage in survival over cells with other phenotypes [31]. PPARα belongs to the nuclear receptor family, which modulates gene transcription in response to specific endogenous and exogenous ligands, such as FA and fibrates, respectively [64]. Based on our database and microarray analyses, PPARα was found to be upregulated in gastric cancer tissues compared to normal gastric tissues and was negatively correlated with prognosis. Because fenofibrate increases p-AMPK expression, which is upstream of the signaling pathway molecule PPARα, promoting its expression and activity [5].

It is reported that fenofibrate accumulates in mitochondria [15]. In our study, damaged mitochondrial structures and releases apoptotic bodies were evident, showing the pro-apoptotic potential of fenofibrate. Han Dongfeng *et al*. also reported fenofibrate damage to mitochondrial structures [16]. Mitochondrial structural damage could result from oxidative stress, enhanced ROS, and electron influx. Mitochondrial DNA (mtDNA) is essential for the maintenance of functionally competent organelles. The accumulation of mtDNA mutations or decreased mtDNA copy number is expected to cause mitochondrial dysfunction affecting energy generation and cell survival, as these processes have been associated with aging, mitochondrial diseases, and cancer [65-67]. mtDNA alterations mainly include copy number change, point mutations, insertions, and deletions, which were reported to cause malignant transformation in cancers [68]. Most mtDNA point mutations identified in cancer tissues have a high potential to result in mitochondrial dysfunction [69]. This dysfunction, caused by such mtDNA mutations or mitochondrial enzyme defects, not only perturbs cellular bioenergetics toward metabolic reprogramming in cancer cells, but also triggers tumor-promoting changes mediated by ROS, Ca^{2+}, or small molecule metabolites released by mitochondria [69]. In gastric cancers, mtDNA copy number is lower than normal gastric tissue [70]. After fenofibrate treatment, we found mtDNA content was reduced. Decreasing mtDNA could make gas-

tric cancer cells more vulnerable by attenuating mitochondrial function and cutting off the energy supply to inhibit cell growth. HK2 and PFK activity in MGC803 and SGC7901 cells significantly decreased after fenofibrate treatment. HK2 dissociation from the mitochondria via the promotion of VDAC1 oligomerization, contributing to mPTP opening and cytochrome-c release, activates Caspase-9-dependent cellular apoptosis [71].

PPARα upregulation was thought to be a feedback response to fenofibrate treatment. Some studies have shown that the anti-tumor effects of fenofibrate are dependent on the PPARα pathway. Han *et al*. found that fenofibrate induced cell cycle arrest in U87MG cells during the G0/G1 phase [23]. Pretreatment of U87MG cells with PPARα siRNA significantly rescued fenofibrate-induced cell cycle arrest, suggesting that fenofibrate induced G0/G1 arrest by PPARα-dependent mechanisms [23]. We found that down-regulation of PPARα decreased cell apoptosis induced by fenofibrate and increased cell proliferation and colony formation of gastric cancer cells, which were attenuated by fenofibrate. Importantly, our results demonstrate that some fenofibrate anti-tumor mechanisms are partially depended on PPARα, since PPARα siRNA pretreatment compromised fenofibrate's effects on mitochondrial function and metabolism.

In addition to anti-tumor effects *in vitro*, fenofibrate was show to be effective *in vivo* with no obvious side effects. Through intragastric administration imitating human oral use, fenofibrate impeded subcutaneous xenograft tumor growth without significant hepatic, renal, or systematic toxicities. Other studies have also confirmed the effectiveness and safety of fenofibrate *in vivo* [8, 25]. Immunohistochemical analysis and Tunnel staining showed fenofibrate inhibited proliferation, glycolysis, and FFA synthesis-related molecular expression while increasing the percentage of apoptotic cells and pro-apoptosis and FFA catabolism-related molecular signatures, indicating the mechanisms of tumor inhibition by fenofibrate. Increased SOD2 expression indicates that the oxidative stress induced by fenofibrate in gastric xenografts is consistent with *in vitro* results.

In conclusion, we demonstrate that fenofibrate exerts anti-tumor activity both *in vivo* and *in vitro* by inducing a reversal in cell metabolism and causing mitochondrial dysfunction, which could potentially form a new anti-tumor strategy in cancer treatment. PPARα was highly expressed in gastric cancer tissues and regulates the anti-tumor effects of fenofibrate in gastric cancer, supporting PPARα as a therapeutic target and prognosticator of gastric cancer. Some studies have suggested a combination of first-line therapeutic agents and mitochondrial targeting agents could plausibly serve as an effective strategy to curtail tumor progression [49]. The promising results of this investigation support further exploration into combining fenofibrate with other therapies to strengthen cancer treatments.

Acknowledgements

This work was supported by the Natural Science Foundation of China (Grant Number 81172129, 81773238 and 81903136).

Disclosure of conflict of interest

None.

Address correspondence to: Hui Xu and Fuxiang Zhou, Department of Radiation and Medical Oncology, Zhongnan Hospital of Wuhan University, Wuhan 430071, China; Hubei Province Key Laboratory of Tumor Biological Behaviors, Wuhan 430071, China; Hubei Cancer Clinical Study Center, Wuhan 430071, China. Tel: +86-18871483029; E-mail: xuhui@whu.edu.cn (HX); Tel: +86-276781-3155; E-mail: happyzhoufx@sina.com (FXZ)

References

[1] Currie E, Schulze A, Zechner R, Walther TC and Farese RV Jr. Cellular fatty acid metabolism and cancer. Cell Metab 2013; 18: 153-161.
[2] Pavlova NN and Thompson CB. The emerging hallmarks of cancer metabolism. Cell Metab 2016; 23: 27-47.
[3] Zong WX, Rabinowitz JD and White E. Mitochondria and cancer. Mol Cell 2016; 61: 667-676.
[4] Luengo A, Gui DY and Vander Heiden MG. Targeting metabolism for cancer therapy. Cell Chem Biol 2017; 24: 1161-1180.
[5] Grabacka M and Reiss K. Anticancer properties of PPARalpha-effects on cellular metabolism and inflammation. PPAR Res 2008; 2008: 930705.
[6] Egerod FL, Nielsen HS, Iversen L, Thorup I, Storgaard T and Oleksiewicz MB. Biomarkers

for early effects of carcinogenic dual-acting PPAR agonists in rat urinary bladder urothelium in vivo. Biomarkers 2005; 10: 295-309.
[7] Grabacka M, Placha W, Plonka PM, Pajak S, Urbanska K, Laidler P and Slominski A. Inhibition of melanoma metastases by fenofibrate. Arch Dermatol Res 2004; 296: 54-58.
[8] Panigrahy D, Kaipainen A, Huang S, Butterfield CE, Barnés CM, Fannon M, Laforme AM, Chaponis DM, Folkman J and Kieran MW. PPARalpha agonist fenofibrate suppresses tumor growth through direct and indirect angiogenesis inhibition. Proc Natl Acad Sci U S A 2008; 105: 985-990.
[9] Saidi SA, Holland CM, Charnock-Jones DS and Smith SK. In vitro and in vivo effects of the PPAR-alpha agonists fenofibrate and retinoic acid in endometrial cancer. Mol Cancer 2006; 5: 13.
[10] Yanae M, Tsubaki M, Satou T, Itoh T, Imano M, Yamazoe Y and Nishida S. Statin-induced apoptosis via the suppression of ERK1/2 and Akt activation by inhibition of the geranylgeranyl-pyrophosphate biosynthe-sis in glioblastoma. J Exp Clin Cancer Res 2011; 30: 74.
[11] Gardette V, Bongard V, Dallongeville J, Arveiler D, Bingham A, Ruidavets JB, Amouyel P, Haas B, Ducimetière P and Ferrières J. Ten-year all-cause mortality in presumably healthy subjects on lipid-lowering drugs (from the Prospective Epidemiological Study of Myocar-dial Infarction [PRIME] prospective cohort). Am J Cardiol 2009; 103: 381-386.
[12] Staels B, Dallongeville J, Auwerx J, Schoonjans K, Leitersdorf E and Fruchart JC. Mechanism of action of fibrates on lipid and lipoprotein metabolism. Circulation 1998; 98: 2088-2093.
[13] Srivastava RA. Fenofibrate ameliorates diabetic and dyslipidemic profiles in KKAy mice partly via down-regulation of 11beta-HSD1, PEPCK and DGAT2. Comparison of PPARalpha, PPARgamma, and liver x receptor agonists. Eur J Pharmacol 2009; 607: 258-263.
[14] Pettersen JC, Pruimboom-Brees I, Francone OL, Amacher DE, Boldt SE, Kerlin RL and Ballinger WE. The PPARalpha agonists fenofibrate and CP-778875 cause increased beta-oxidation, leading to oxidative injury in skeletal and cardiac muscle in the rat. Toxicol Pathol 2012; 40: 435-447.
[15] Wilk A, Wyczechowska D, Zapata A, Dean M, Mullinax J, Marrero L, Parsons C, Peruzzi F, Culicchia F, Ochoa A, Grabacka M and Reiss K. Molecular mechanisms of fenofibrate-induced metabolic catastrophe and glioblastoma cell death. Mol Cell Biol 2015; 35: 182-198.
[16] Han D, Wei W, Chen X, Zhang Y, Wang Y, Zhang J, Wang X, Yu T, Hu Q, Liu N and You Y. NF-kappaB/RelA-PKM2 mediates inhibition of glycolysis by fenofibrate in glioblastoma cells. Oncotarget 2015; 6: 26119-26128.
[17] Su C, Shi A, Cao G, Tao T, Chen R, Hu Z, Shen Z, Tao H, Cao B, Hu D and Bao J. Fenofibrate suppressed proliferation and migration of human neuroblastoma cells via oxidative stress dependent of TXNIP upregulation. Biochem Biophys Res Commun 2015; 460: 983-988.
[18] Binello E, Mormone E, Emdad L, Kothari H and Germano IM. Characterization of fenofibrate-mediated anti-proliferative pro-apoptotic effects on high-grade gliomas and anti-invasive effects on glioma stem cells. J Neurooncol 2014; 117: 225-234.
[19] Liang H, Kowalczyk P, Junco JJ, Klug-De Santiago HL, Malik G, Wei SJ and Slaga TJ. Differential effects on lung cancer cell proliferation by agonists of glucocorticoid and PPARalpha receptors. Mol Carcinog 2014; 53: 753-763.
[20] Zhao H, Zhu C, Qin C, Tao T, Li J, Cheng G, Li P, Cao Q, Meng X, Ju X, Shao P, Hua L, Gu M and Yin C. Fenofibrate down-regulates the expressions of androgen receptor (AR) and AR target genes and induces oxidative stress in the prostate cancer cell line LNCaP. Biochem Biophys Res Commun 2013; 432: 320-325.
[21] Yamasaki D, Kawabe N, Nakamura H, Tachibana K, Ishimoto K, Tanaka T, Aburatani H, Sakai J, Hamakubo T, Kodama T and Doi T. Fenofibrate suppresses growth of the human hepatocellular carcinoma cell via PPARalpha-independent mechanisms. Eur J Cell Biol 2011; 90: 657-664.
[22] Zhang KL, Han L, Chen LY, Shi ZD, Yang M, Ren Y, Chen LC, Zhang JX, Pu PY and Kang CS. Blockage of a miR-21/EGFR regulatory feedback loop augments anti-EGFR therapy in glioblastomas. Cancer Lett 2014; 342: 139-149.
[23] Han DF, Zhang JX, Wei WJ, Tao T, Hu Q, Wang YY, Wang XF, Liu N and You YP. Fenofibrate induces G0/G1 phase arrest by modulating the PPARalpha/FoxO1/p27 kip pathway in human glioblastoma cells. Tumour Biol 2015; 36: 3823-3829.
[24] Huang YC, Liu KC, Chiou YL, Yang CH, Chen TH, Li TT and Liu LL. Fenofibrate suppresses melanogenesis in B16-F10 melanoma cells via activation of the p38 mitogen-activated protein kinase pathway. Chem Biol Interact 2013; 205: 157-164.
[25] Li T, Zhang Q, Zhang J, Yang G, Shao Z, Luo J, Fan M, Ni C, Wu Z and Hu X. Fenofibrate induces apoptosis of triple-negative breast cancer cells via activation of NF-kappaB pathway. BMC Cancer 2014; 14: 96.
[26] Piwowarczyk K, Wybieralska E, Baran J, Borowczyk J, Rybak P, Kosińska M, Włodarczyk AJ, Michalik M, Siedlar M, Madeja Z, Dobrucki J,

Reiss K and Czyż J. Fenofibrate enhances barrier function of endothelial continuum within the metastatic niche of prostate cancer cells. Expert Opin Ther Targets 2015; 19: 163-176.
[27] Leung DTH and Chu S. Measurement of oxidative stress: mitochondrial function using the seahorse system. Methods Mol Biol 2018; 1710: 285-293.
[28] Wallace DC, Fan W and Procaccio V. Mitochondrial energetics and therapeutics. Annu Rev Pathol 2010; 5: 297-348.
[29] Galluzzi L, Kepp O and Kroemer G. Mitochondria: master regulators of danger signaling. Nat Rev Mol Cell Biol 2012; 13: 780-788.
[30] Yan Y, Xu H, Zhang L, Qian X, Zhou J, Huang Y, Ge W and Wang W. RRAD suppresses the Warburg effect by downregulating ACTG1 in hepatocellular carcinoma. Onco Targets Ther 2019; 12: 1691-1703.
[31] Yu L, Lu M, Jia D, Ma J, Ben-Jacob E, Levine H, Kaipparettu BA and Onuchic JN. Modeling the genetic regulation of cancer metabolism: interplay between glycolysis and oxidative phosphorylation. Cancer Res 2017; 77: 1564-1574.
[32] Bray F, Ferlay J, Soerjomataram I, Siegel RL, Torre LA and Jemal A. Global cancer statistics 2018: GLOBOCAN estimates of incidence and mortality worldwide for 36 cancers in 185 countries. CA Cancer J Clin 2018; 68: 394-424.
[33] Ajani JA, Lee J, Sano T, Janjigian YY, Fan D and Song S. Gastric adenocarcinoma. Nat Rev Dis Primers 2017; 3: 17036.
[34] Hanahan D and Weinberg RA. Hallmarks of cancer: the next generation. Cell 2011; 144: 646-674.
[35] Cuezva JM, Krajewska M, de Heredia ML, Krajewski S, Santamaría G, Kim H, Zapata JM, Marusawa H, Chamorro M and Reed JC. The bioenergetic signature of cancer: a 311 marker of tumor progression. Cancer Res 2002; 62: 6674-6681.
[36] Medes G, Thomas A and Weinhouse S. Metabolism of neoplastic tissue. IV. A study of lipid synthesis in neoplastic tissue slices in vitro. Cancer Res 1953; 13: 27-29.
[37] Ookhtens M, Kannan R, Lyon I and Baker N. Liver and adipose tissue contributions to newly formed fatty acids in an ascites tumor. Am J Physiol 1984; 247: R146-R153.
[38] Röhrig F and Schulze A. The multifaceted roles of fatty acid synthesis in cancer. Nat Rev Cancer 2016; 16: 732-749.
[39] Kuhajda FP, Jenner K, Wood FD, Hennigar RA, Jacobs LB, Dick JD and Pasternack GR. Fatty acid synthesis: a potential selective target for antineoplastic therapy. Proc Natl Acad Sci U S A 1994; 91: 6379-6383.
[40] Menendez JA and Lupu R. Oncogenic properties of the endogenous fatty acid metabolism: molecular pathology of fatty acid synthase in cancer cells. Curr Opin Clin Nutr Metab Care 2006; 9: 346-357.
[41] Toyokuni S, Okamoto K, Yodoi J and Hiai H. Persistent oxidative stress in cancer. FEBS Lett 1995; 358: 1-3.
[42] Papa L and Germain D. SirT3 regulates the mitochondrial unfolded protein response. Mol Cell Biol 2014; 34: 699-710.
[43] Yun CH, Bae CS and Ahn T. Cargo-free nanoparticles containing cationic-lipids induce reactive oxygen species and cell death in HuH7 cells. Biol Pharm Bull 2016; 39: 1338-1346.
[44] Yun CH, Bae CS and Ahn T. Cationic nanoparticles containing cationic peptide cargo synergistically induce cellular reactive oxygen species and cell death in HuH7 cells. Int J Pept Res Ther 2019; 25: 323-327.
[45] Sena LA and Chandel NS. Physiological roles of mitochondrial reactive oxygen species. Mol Cell 2012; 48: 158-167.
[46] Zhang Y and Martin SG. Redox proteins and radiotherapy. Clin Oncol (R Coll Radiol) 2014; 26: 289-300.
[47] Jeon JH, Kim DK, Shin Y, Kim HY, Song B, Lee EY, Kim JK, You HJ, Cheong H, Shin DH, Kim ST, Cheong JH, Kim SY and Jang H. Migration and invasion of drug-resistant lung adenocarcinoma cells are dependent on mitochondrial activity. Exp Mol Med 2016; 48: e277.
[48] Burke PJ. Mitochondria, bioenergetics and apoptosis in cancer. Trends Cancer 2017; 3: 857-870.
[49] Viale A, Corti D and Draetta GF. Tumors and mitochondrial respiration: a neglected connection. Cancer Res 2015; 75: 3685-3686.
[50] Zhou H, Zhang B, Zheng J, Yu M, Zhou T, Zhao K, Jia Y, Gao X, Chen C and Wei T. The inhibition of migration and invasion of cancer cells by graphene via the impairment of mitochondrial respiration. Biomaterials 2014; 35: 1597-1607.
[51] Kalainayakan SP, FitzGerald KE, Konduri PC, Vidal C and Zhang L. Essential roles of mitochondrial and heme function in lung cancer bioenergetics and tumorigenesis. Cell Biosci 2018; 8: 56.
[52] Xu H, Ma J, Wu J, Chen L, Sun F, Qu C, Zheng D and Xu S. Gene expression profiling analysis of lung adenocarcinoma. Braz J Med Biol Res 2016; 49.
[53] Vatrinet R, Iommarini L, Kurelac I, De Luise M, Gasparre G and Porcelli AM. Targeting respiratory complex I to prevent the Warburg effect. Int J Biochem Cell Biol 2015; 63: 41-45.
[54] Jara JA and Lopez-Munoz R. Metformin and cancer: between the bioenergetic disturbanc-

es and the antifolate activity. Pharmacol Res 2015; 101: 102-108.
[55] Alam MM, Sohoni S, Kalainayakan SP, Garrossian M and Zhang L. Cyclopamine tartrate, an inhibitor of hedgehog signaling, strongly interferes with mitochondrial function and suppresses aerobic respiration in lung cancer cells. BMC Cancer 2016; 16: 150.
[56] Ellinghaus P, Heisler I, Unterschemmann K, Haerter M, Beck H, Greschat S, Ehrmann A, Summer H, Flamme I, Oehme F, Thierauch K, Michels M, Hess-Stumpp H and Ziegelbauer K. BAY 87-2243, a highly potent and selective inhibitor of hypoxia- induced gene activation has antitumor activities by inhibition of mitochondrial complex I. Cancer Med 2013; 2: 611-624.
[57] Tomasetti M, Nocchi L, Staffolani S, Manzella N, Amati M, Goodwin J, Kluckova K, Nguyen M, Strafella E, Bajzikova M, Peterka M, Lettlova S, Truksa J, Lee W, Dong LF, Santarelli L and Neuzil J. MicroRNA-126 suppresses mesothelioma malignancy by targeting IRS1 and interfering with the mitochondrial function. Antioxid Redox Signal 2014; 21: 2109-2125.
[58] Andrzejewski S, Gravel SP, Pollak M, Tomasetti M, Nocchi L, Staffolani S, Manzella N, Amati M, Goodwin J, Kluckova K, Nguyen M, Strafella E, Bajzikova M, Peterka M, Lettlova S, Truksa J, Lee W, Dong LF, Santarelli L and Neuzil J. Metformin directly acts on mitochondria to alter cellular bioenergetics. Cancer Metab 2014; 21: 2109-2025.
[59] Janzer A, German NJ, Gonzalez-Herrera KN, Asara JM, Haigis MC and Struhl K. Metformin and phenformin deplete tricarboxylic acid cycle and glycolytic intermediates during cell transformation and NTPs in cancer stem cells. Proc Natl Acad Sci U S A 2014; 111: 10574-10579.
[60] Liu X, Romero IL, Litchfield LM, Lengyel E and Locasale JW. Metformin targets central carbon metabolism and reveals mitochondrial requirements in human cancers. Cell Metab 2016; 24: 728-739.
[61] Schneider MB, Matsuzaki H, Haorah J, Ulrich A, Standop J, Ding XZ, Adrian TE and Pour PM. Prevention of pancreatic cancer induction in hamsters by metformin. Gastroenterology 2001; 120: 1263-1270.
[62] Mayer IA and Arteaga CL. The PI3K/AKT pathway as a target for cancer treatment. Annu Rev Med 2016; 67: 11-28.
[63] Faubert B, Boily G, Izreig S, Griss T, Samborska B, Dong Z, Dupuy F, Chambers C, Fuerth BJ and Viollet B. AMPK is a negative regulator of the Warburg effect and suppresses tumor growth in vivo. Cell Metab 2013; 17: 113-124.
[64] Huang J, Das SK, Jha P, Al Zoughbi W, Schauer S, Claudel T, Sexl V, Vesely P, Birner-Gruenberger R, Kratky D, Trauner M and Hoefler G. The PPARα agonist fenofibrate suppresses B-cell lymphoma in mice by modulating lipid metabolism. Biochim Biophys Acta 2013; 1831: 1555-1565.
[65] Wallace DC. Mitochondria and cancer. Nat Rev Cancer 2012; 12: 685-698.
[66] Wallace DC. A mitochondrial bioenergetic etiology of disease. J Clin Invest 2013; 123: 1405-1412.
[67] Lee HC, Chang CM and Chi CW. Somatic mutations of mitochondrial DNA in aging and cancer progression. Ageing Res Rev 2010; 9 Suppl 1: S47-58.
[68] Larsen NB, Rasmussen M and Rasmussen LJ. Nuclear and mitochondrial DNA repair: similar pathways? Mitochondrion 2005; 5: 89-108.
[69] Hsu CC, Tseng LM and Lee HC. Role of mitochondrial dysfunction in cancer progression. Exp Biol Med (Maywood) 2016; 241: 1281-1295.
[70] Wu CW, Yin PH, Hung WY, Li AF, Li SH, Chi CW, Wei YH and Lee HC. Mitochondrial DNA mutations and mitochondrial DNA depletion in gastric cancer. Genes Chromosomes Cancer 2005; 44: 19-28.
[71] Zhou H, Hu S, Jin Q, Shi C, Zhang Y, Zhu P, Ma Q, Tian F and Chen Y. Mff-dependent mitochondrial fission contributes to the pathogenesis of cardiac microvasculature ischemia/reperfusion injury via induction of mROS-mediated cardiolipin oxidation and HK2/VDAC1 disassociation-involved mPTP opening. J Am Heart Assoc 2017; 6.

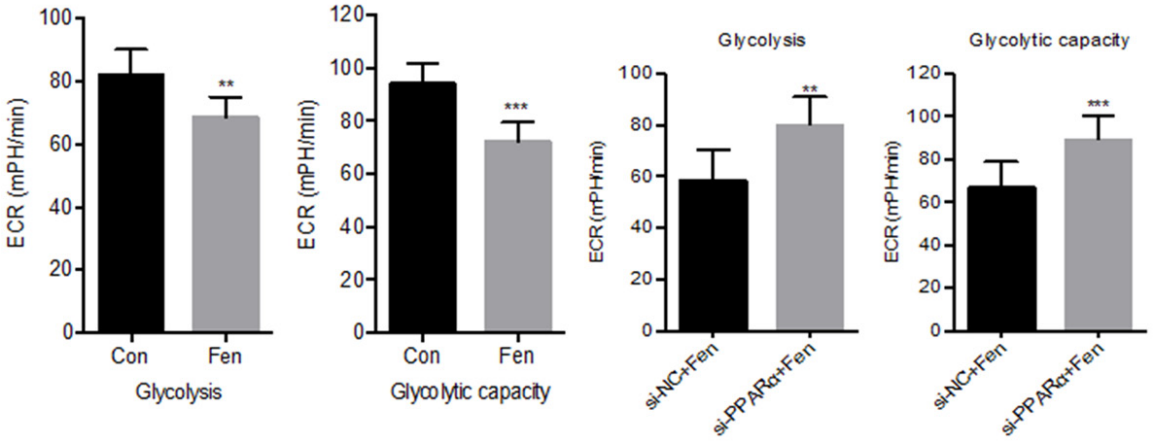

Figure S1. The extracellular acidification rate (ECAR) determined by the Seahorse XF24 analyzer in MGC803 cells with or without fenofibrate treatment. The glycolytic level and glycolysis capacity were calculated from seahorse analysis. PPARα si-RNA interference restored the reduced glycolysis by fenofibrate in MGC803 cells.

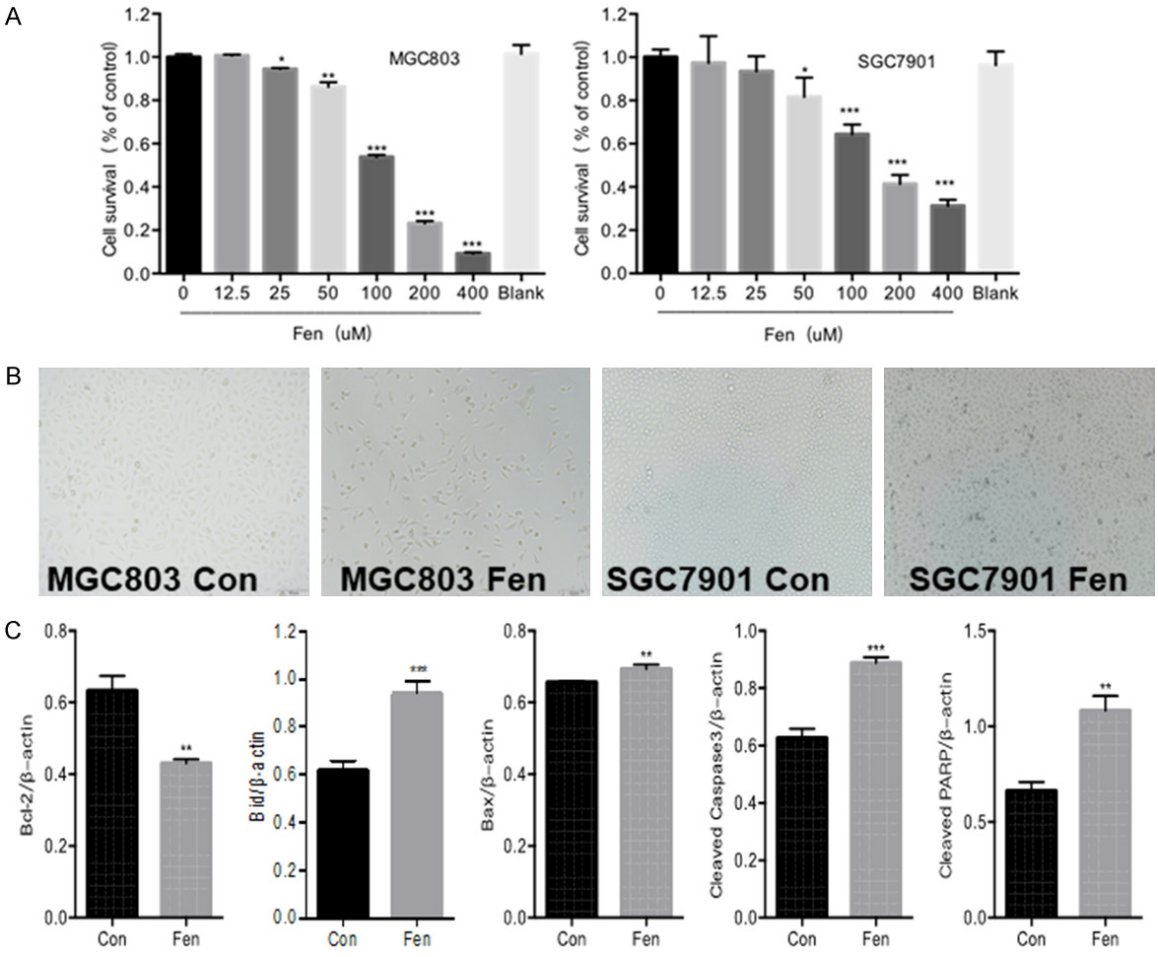

Figure S2. A. Effects of different concentrations of fenofibrate treatment for 24 hours on the cell survival of MGC803 and SGC7901 cells. B. Fenofibrate treatment reduced cell density and changed cell morphology. C. Western blot was used to detect the apoptosis-related proteins Bcl-2, Bid, Bax, Caspase3 and PARP protein expression in the control group and fenofibrate treatment group. The gray values of the bands were measured.

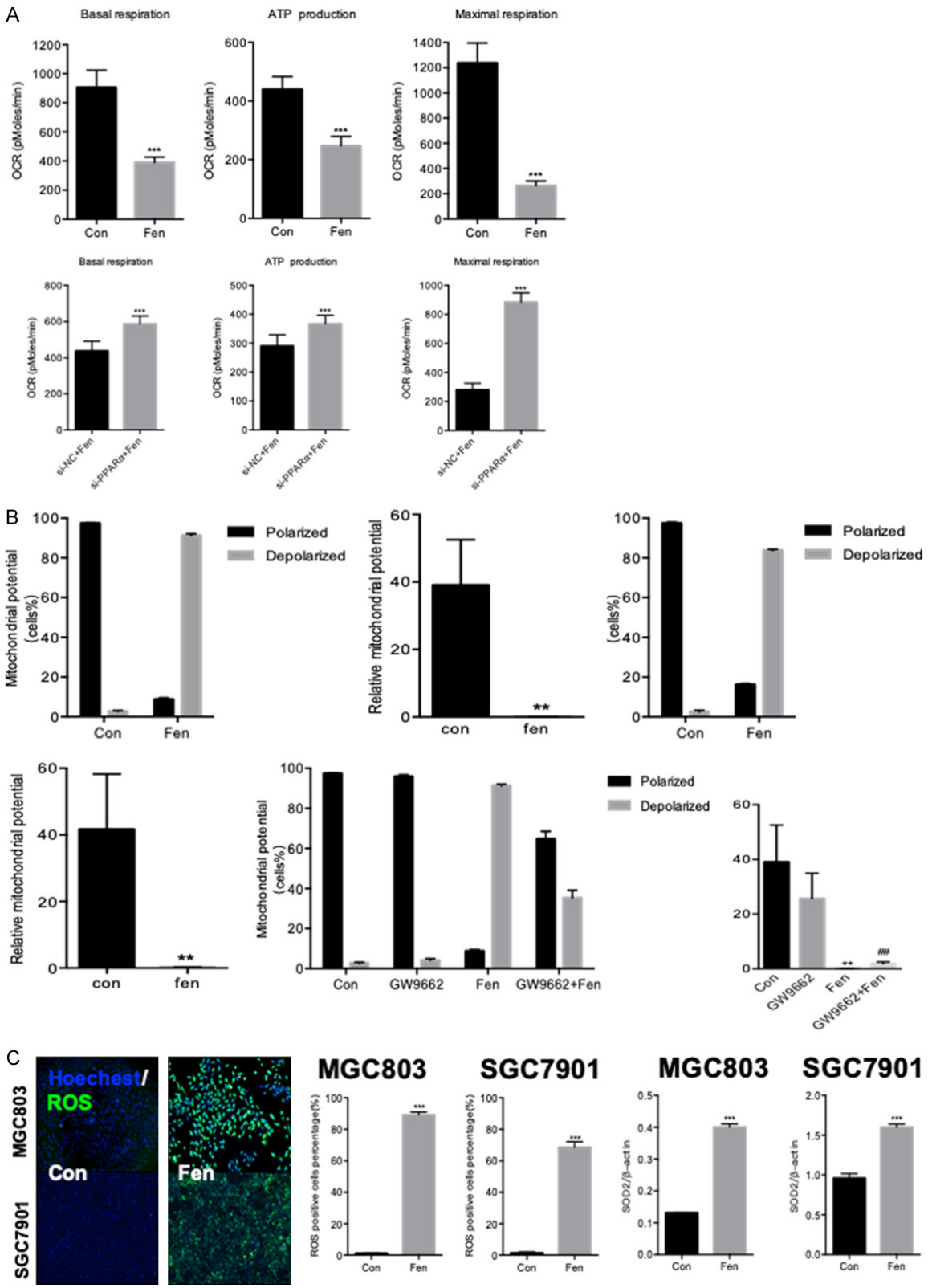

Figure S3. A. The oxygen consumption rate (OCR) determined by the Seahorse XF24 analyser in MGC803 cells with or without fenofibrate treatment. Basal respiration level, ATP production and maximal respiration level were calculated from the seahorse analysis. B. After fenofibrate treatment, the mitochondria of MGC803 cells and SGC7901 cells were depolarized, and the mitochondrial membrane potential decreased. C. Effects of fenofibrate on ROS production and SOD2 levels in gastric cancer MGC803 and SGC7901 cells. The gray values of the bands were measured.

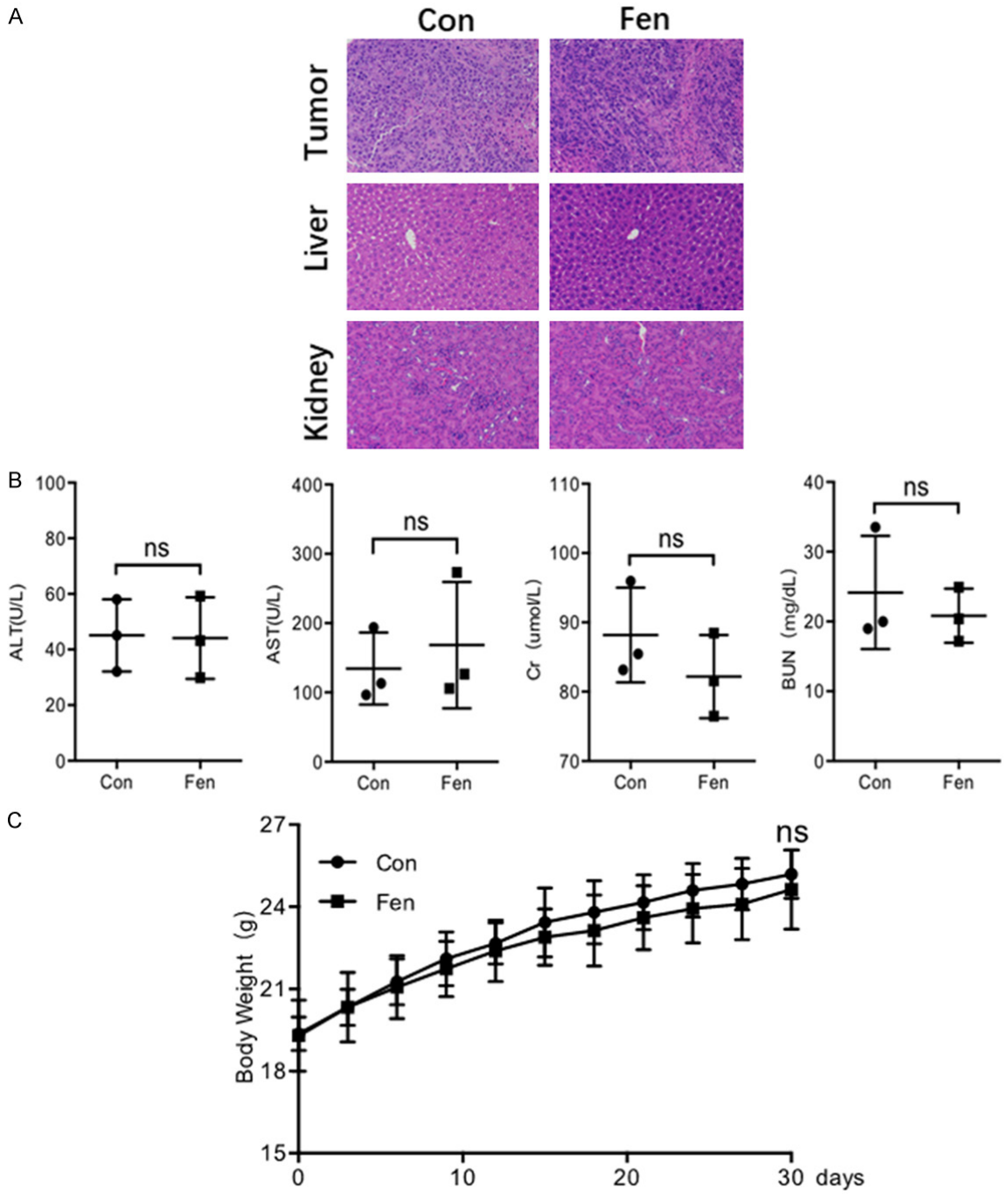

Figure S4. A. H&E staining of tumor tissues, livers and kidneys. B. The concentrations of alanine aminotransferase (ALT), aspartate aminotransferase (AST), creatinine (Cr) and urea nitrogen (BUN) in the blood were not statistically significant between the control group and fenofibrate treatment group. C. The body weights had no significant difference between the control group and the fenofibrate treatment group.